

Ore minerals and geochemical characterization of the Dungash gold deposit, South Eastern Desert, Egypt

Islam A. Dourgham¹ · Khairiya M. Fawzy² · Hartwig E. Frimmel³

Received: 15 May 2016 / Accepted: 9 February 2017 / Published online: 20 March 2017
© Saudi Society for Geosciences 2017

Abstract The Dungash historic gold mine is located in the South Eastern Desert of Egypt. The gold-bearing quartz veins are hosted by the metavolcanic and metavolcaniclastic rocks along an ENE–WSW trending shear zone. Alteration types recorded in the wall rocks are sericitization, silicification, carbonatization, chloritization, sulfidization, ferruginization, and listwanitization. The ore mineral assemblage comprises arsenopyrite, pyrite, native gold, pyrrhotite, sphalerite, chalcopyrite, and galena. The primary sulfide mineral assemblage formed during a hypogene hydrothermal stage whereas angleite and goethite occur as secondary supergene phases. Microthermometric fluid inclusion analysis revealed that the auriferous quartz precipitated from a moderately saline (5 to 11.22 wt% NaCl_{equiv.}) solution at temperatures above the recorded homogenization temperatures (T_h), which range from 380 to 177 °C. The minimum pressures of trapping are between 350 and 400 bars. The fluid evolution during mineralization is explained by mixing of a magmatic fluid with meteoric waters. Initially, the high temperature and moderately saline magmatic fluid dominated and progressively became diluted with meteoric waters. Highest gold content is recorded in the carbonatized zone and the quartz veins. However, gold content in the carbonatized zone of the footwall exceeds

several times its content in the quartz veins and the carbonatized zone of the hanging wall.

Keywords Dungash gold mineralization · Ore minerals · Fluid inclusions · Eastern Desert · Egypt

Introduction

The Dungash gold deposit is located in the South Eastern Desert of Egypt at 24° 56' 03" N and 33° 51' 59" E (Fig. 1). The deposit has been described as an auriferous quartz vein system that cuts metavolcaniclastic rocks of andesitic calc-alkaline affinity within a former volcanic arc rocks (Marten 1986). Ore grades of 0.3 to 5.3 g/t Au were recorded in the alteration zones (Abdel-Tawab 1992). Takla (2001) classified the Dungash gold mineralization as disseminated gold in sheared and altered volcaniclastic rocks within a volcanic arc. According to Helba et al. (2001), the Dungash area is covered by Pan-African Late Proterozoic rock units comprising an ophiolitic sequence of serpentinite and related talc-carbonate rocks an island arc metavolcaniclastic assemblage (meta-andesite, schist, and metavolcaniclastic rocks) and Cordilleran-type plutonic rocks, all of which are cut by basic and/or acidic dykes (Fig. 1). Helba et al. (2001) recorded several distinctive sericitized zones in the wall rocks, that is, quartz-sericite (at the contact of the mineralized quartz vein followed outward by zones of sericite, carbonate-sericite, and chlorite-sericite. The amount of ore mineral assemblage increases from the sericite zone to the carbonate-sericite zone. Arsenopyrite, pyrite, native gold, and carbonates represent several generations. Khalil et al. (2003) estimated the temperature of formation of these hydrothermal minerals as between 500 and 300 °C. Zoheir et al. (2008) concluded that Dungash is an orogenic, mesothermal gold deposit where gold occurs in

✉ Khairiya M. Fawzy
khairiyafawzy@yahoo.com; fawzik20@gmail.com

¹ Geology Department, Faculty of Science, Al-Azhar University, Nasr City, Cairo, Egypt

² Geology Department, Faculty of Science, Aswan University, Aswan, Egypt

³ Geodynamics and Geomaterials Research Division, Institute of Geography and Geology, University of Wuerzburg, Am Hubland, 97074 Würzburg, Germany

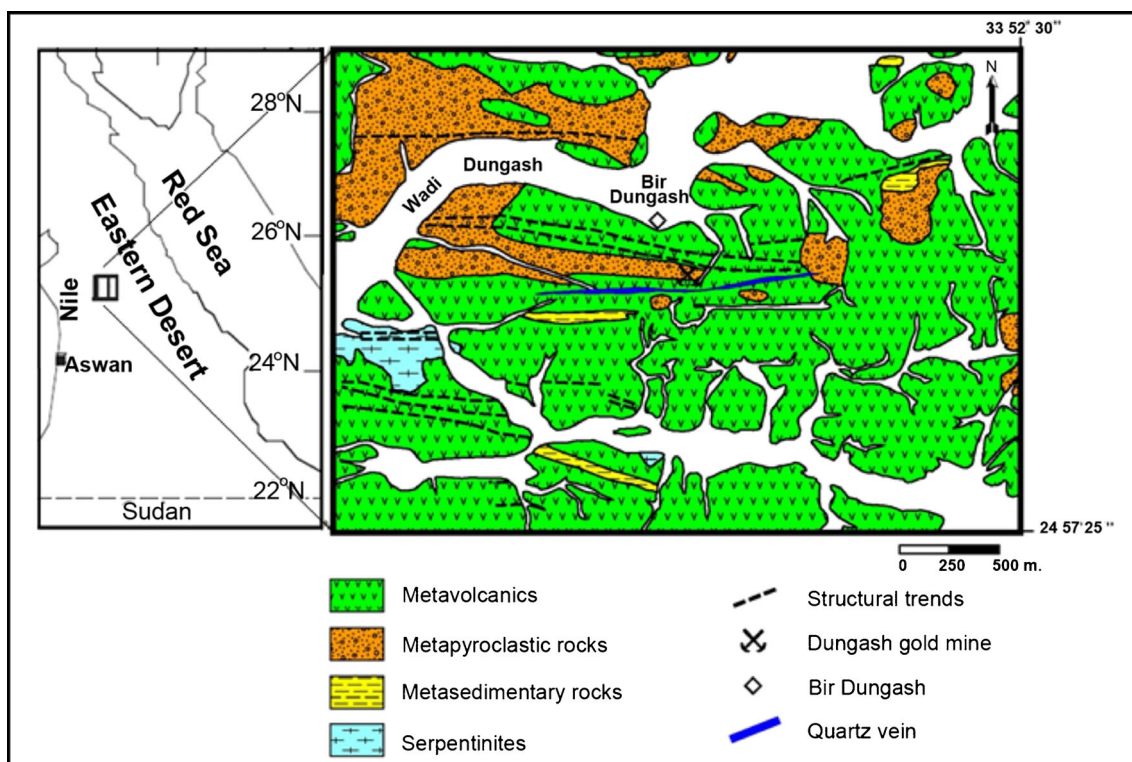


Fig. 1 Geologic map of Dungash gold mine area (after Helba et al. (2001))

shear-related quartz veins or altered (typically carbonatized) greenschist facies host rocks. The precipitation of gold was triggered by reactions between fluid in the shear zones and the metavolcanic/metavolcaniclastic country rock at temperatures of ~300 to 400 °C. Ahmed (2012) used the remote sensing data to detect the alteration zones and map alteration minerals as a guide for gold exploration at Dungash gold mine. Zoheir and Weihed (2014) stated that the host metavolcanic/metavolcaniclastic rocks are commonly with andesitic composition derived from a low-K, calc–alkaline magma in a subduction-related, volcanic arc setting and suggested a mainly metamorphic source for ore fluids at Dungash gold deposit.

The present work addresses the geothermometry, mineralogy, and paragenetic relations of the Dungash gold mineralization and discusses the composition, nature, and origin of mineralizing fluids as well as distribution of gold and associated elements in the mineralized zone. This study is based on detailed petrographical, mineralogical, fluid inclusion, and litho-geochemical studies of the quartz veins and the associated hydrothermal alteration zones.

Geologic field observations

The Dungash gold deposit is hosted by the metavolcanic/metavolcaniclastic rocks, which commonly have andesitic

composition. The metavolcanic rocks are massive to porphyritic. The metavolcaniclastic rocks vary from tuffs to coarse-grained pyroclastics. The gold mineralization is confined to the quartz veins and veinlets cutting through the metavolcanic/metavolcaniclastic rocks (Fig. 2a, b) along a ENE–WSW trending shear zone. The auriferous quartz veins within the shear zone are oriented subparallel to the dominant shear zone foliations and dip to south. The veins are composed chiefly of milky and grey quartz with subordinate amounts of carbonates. The carbonate veins' material locally includes calcite, and/or ankerite, which was weathered to goethite at the exposures, forming rusty brown stains (Fig. 2c). The common vein textures are due to crustiform crystal growth and form vugs partly filled with euhedral quartz and sulfides. The wall rocks of the quartz veins appear fractured and brecciated. Slivers of wall rocks are abundant in the quartz veins. They are rich in disseminated opaque minerals (Fig. 2d).

Hydrothermal alteration processes affected the wall rocks of the quartz veins. The alteration zones show wide variation in color, grain size, structure, and compactness recording remarkable variable action of active hydrothermal fluids. The wall rocks are also enriched in disseminated opaque minerals (Fig. 2e). The opaque minerals are commonly weathered to goethite (Fig. 2f). The main

Fig. 2 **a** Metavolcaniclastic rocks traversed by trench along the main lode (*ML*), looking south. **b** Inclined shaft along the mineralized quartz vein hosted in metavolcaniclastic rocks. **c** Milky quartz vein (underground) with variable carbonate content (*Car*). The carbonate vein material (calcite and/or ankerite) altered to goethite at the exposure forming rusty brown stains (*Gth*). **d** Polished slab of grey quartz showing slivers of wall rock rich in disseminated opaque minerals. **e** Polished slab of metavolcaniclastic rocks showing abundant disseminated opaque minerals. **f** Hand specimen showing milky quartz microvein cutting metavolcaniclastic rocks with abundant disseminated opaque minerals altered to goethite. *G. A. Sul* goethite after pyrite



types of hydrothermal alteration include sericitization, silicification, carbonatization, chloritization, sulfidation, and ferruginization. Brown quartz–carbonate pods (listwanite) are dominant in the samples that were collected from the underground workings. The pods are rich in disseminated opaque minerals (Fig. 3a, b).

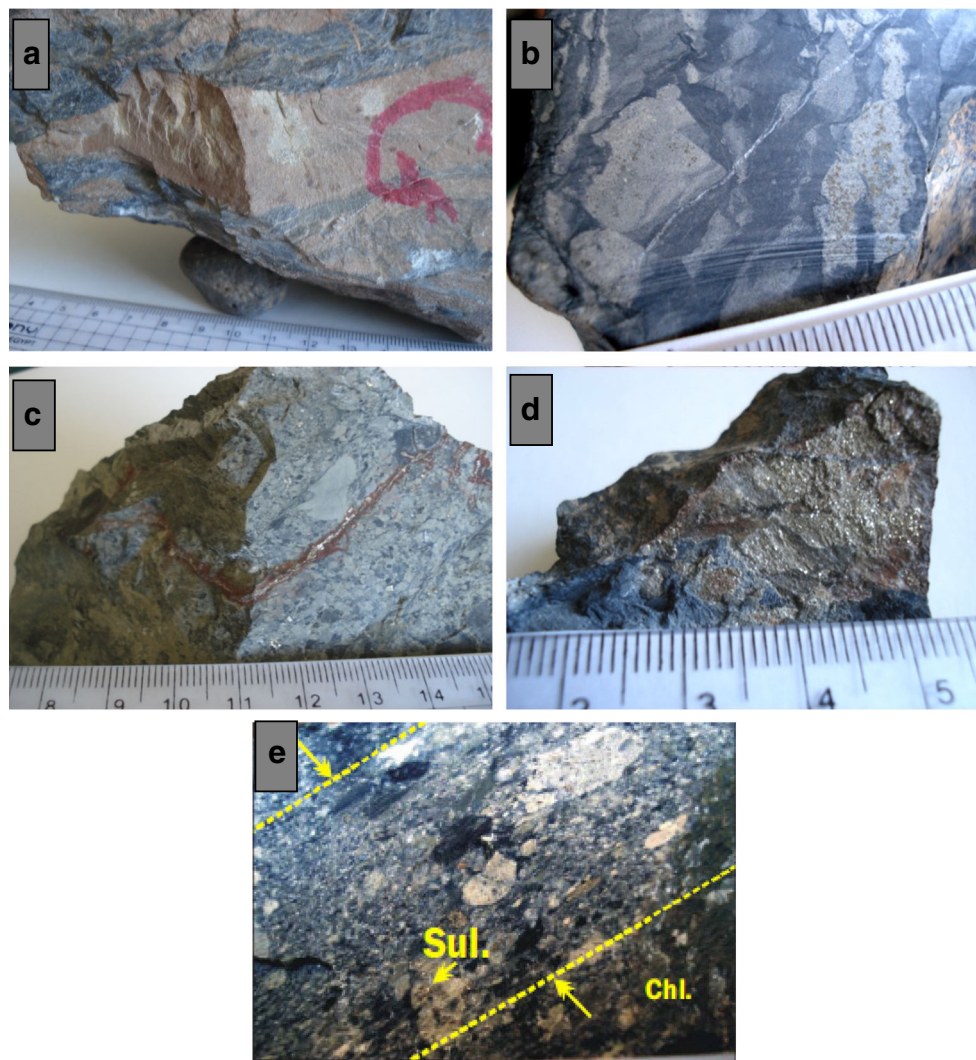
The mine area was affected by brittle–ductile deformation producing shear zones of shallow or steep dip to the south up to 10 m width. Foliation of the metavolcaniclastic rocks, fracturing, and shearing of the wall rocks are the major factors controlling the alteration and the mineralization. These provided favorable channelways for fluid flow (Fig. 3c). Thin and discontinuous microfractures are filled by opaque minerals (Fig. 3c, d). Figure 3c shows sulfide minerals formed along fracture characterized by reddish colored ferruginization due to oxidation of these minerals. Subsequent folding leads to a weak to moderate foliation.

The clastic grains are moderately flattened and arranged in oriented direction indicating compression (Fig. 3e). The predominant fractures and kink microfaults reflect brittle deformation.

Sampling and analytical techniques

Thirty-eight bedrock samples were collected from two profiles arranged perpendicular to the trend of the veins. The distance between samples along profiles is not regular and ranges from 0.5 m for mineralized vein and hydrothermally altered wall rocks to 10–20 m for the least altered distant samples. Moreover, numerous rock samples were collected from dumps at the mouths of the old shafts.

Fig. 3 **a** Hand specimen showing quartz–carbonate (listwanite) pods cutting through the metavolcanic rock and enriched in disseminated opaque minerals. **b** Polished slab showing quartz–carbonate pods rich in disseminated opaque minerals. **c** Hand specimen of metavolcaniclastic rock showing opaque minerals formed along fracture by ferrugination process. **d** Hand specimen showing the opaque mineral filling fracture in the wall rock. **e** Hand specimen of metavolcaniclastic rock showing flattened grains arranged in oriented direction indicating compression



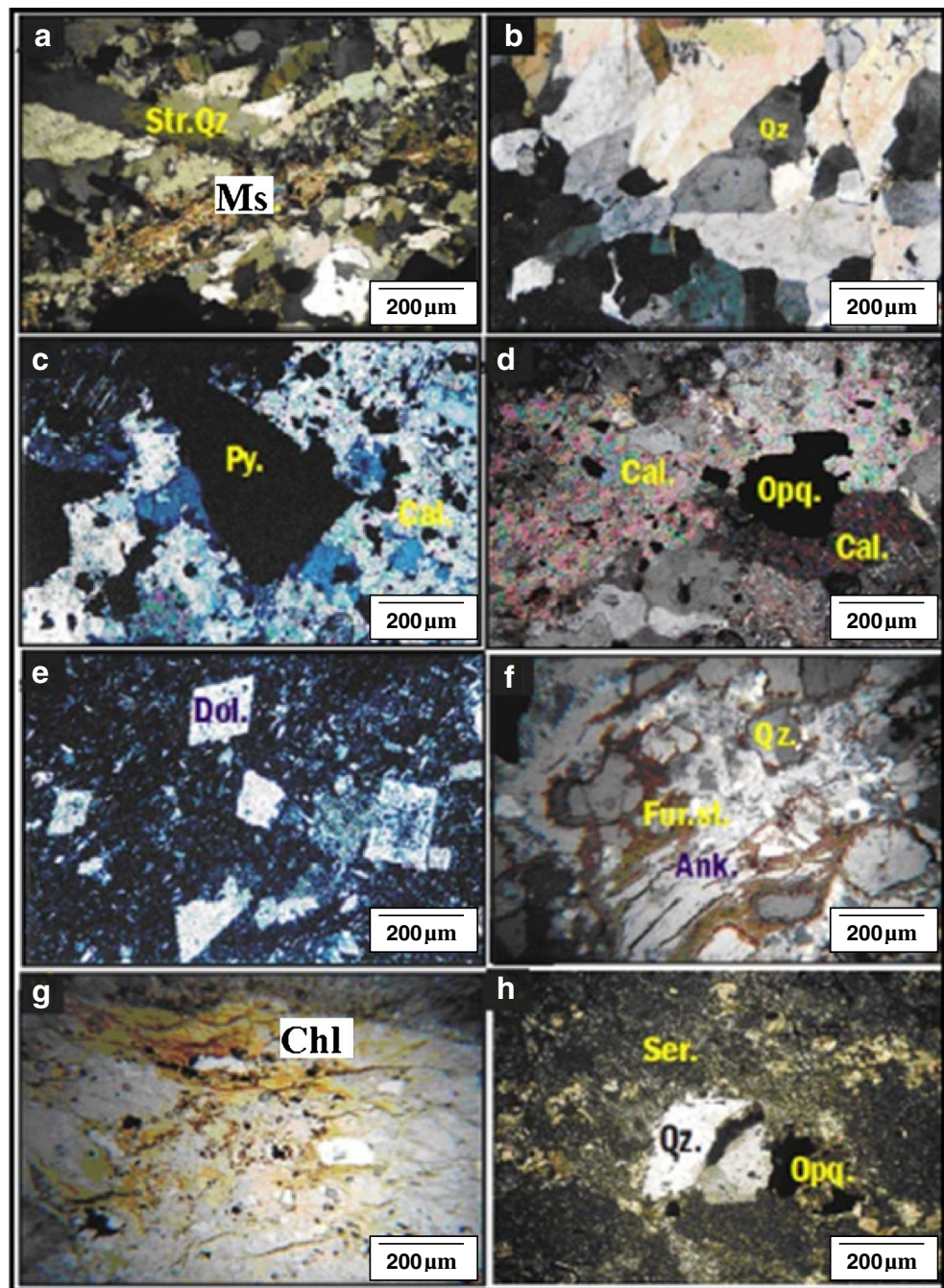
Representative samples were subjected to petrographic and ore microscopic studies. Electron microprobe analysis was carried out at the former Institute of Mineralogy, now the Institute of Geography and Geology, at the University of Würzburg, using aSX-50 CAMECA microprobe operating conditions with 20 kV acceleration voltage, 15 nA beam current, and 20–30 s (sec) counting time. The beam diameter was set at 1 μ for all phases.

Twenty-three samples representing the metavolcanoclastic host rocks and auriferous quartz veins as well as altered wall rock were analyzed for major and trace elements at the National Research Center (NRC) of Egypt, using an a Philips 50 MHz model Pv 8210 inductively coupled plasma atomic emission spectrometry (ICP-AES). Sample digestion of 0.5 g of each sample in Teflon crucible, then 3 ml of perchloric acid, 5 ml of nitric acid, and 15 ml of hydrofluoric acid were added. All crucibles were covered and put on a hot plate for 3 h till complete digestion; then, covers were removed to evaporate silica tetra fluoride till complete evaporation, 5 ml HCl were added to

dissolve the remaining part after digestion till dry, then 50 ml HCl (1:1) were added and wait till complete dissolving and finally, put the dissolved solution in measuring flask (100 ml) and complete up to volume with distilled water. A series of standard volcanic and metavolcanoclastic rock samples was used. Gold analysis was conducted using the fire assay method at the Central Laboratories of the Geological Survey of Egypt.

Microthermometric studies were conducted on gold-bearing quartz vein samples using a USGS gas flow heating/freezing system (USA 1991) at the Department of Earth Resources, Faculty of Engineering, Kyushu University, Japan. Samples were cut into thin slabs using a diamond-edged saw with a slow speed to avoid overheating. From each slab, a doubly polished wafer was produced using standard techniques. From microthermometric results, the following characteristics of fluid inclusions in the auriferous quartz samples were determined: (a) the freezing point depression temperatures, (b) the concentration of solution, (c) the eutectic temperature, (d) the homogenization temperatures, (e) the

Fig. 4 Photomicrographs showing stretched quartz crystals (of silicification) invaded by later acicular sericite crystals (of sericitization) (a), coarse quartz aggregates showing undulose extinction (b), calcite aggregates containing pyrite (c), opaque mineral that occurs within calcite aggregates (d), dolomite rhombohedrons disseminated in the metavolcanoclastic rocks (e), brown rims staining the ankerite grains (f), chlorite flakes filling spaces between the quartz and the carbonate minerals (g), opaque minerals associated with quartz and sericite (h). *Str. Qz* stretch quartz, *Ms* muscovite, *Qz*, quartz, *Py*, pyrite, *Cal* calcite, *Opq.* opaques, *Dol.* dolomite, *Ser.* sericite, *Chl* chlorite, *Fur. St.* ferruginous staining



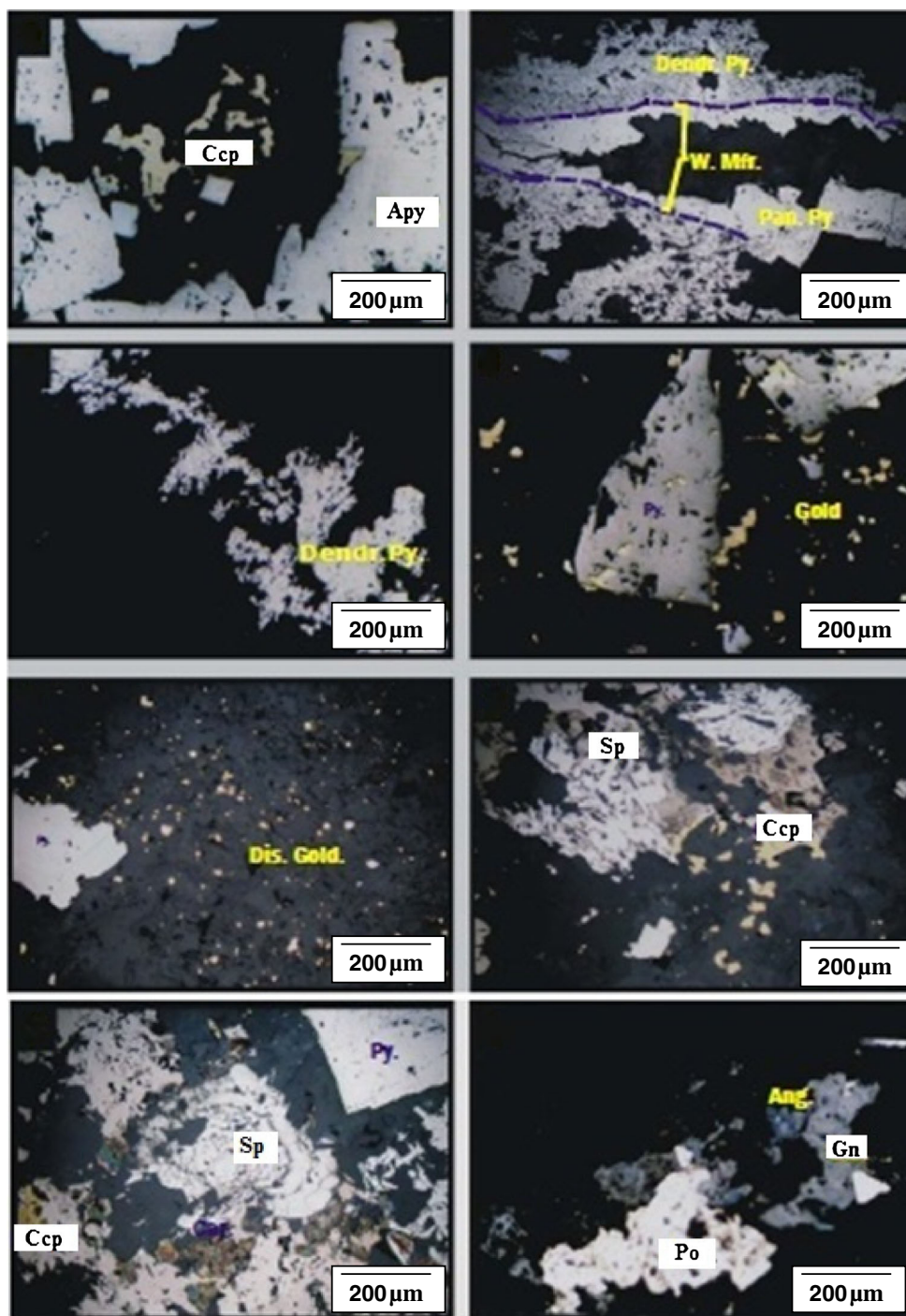
fluid density, and (f) the pressure using the FLINCOR computer program (Brown 1989) and the chemical system described by Zhang and Frantz (1987).

Petrography of the wall rock alteration zones

Alteration types are paragenetically arranged based on their petrographical textural and crosscut relationships as follows:

Silicification is the early alteration type and is represented by elongated stretched quartz crystals invaded by acicular sericite grains and muscovite laths (Fig. 4a). Quartz occurs as coarse-grained subhedral crystal aggregates showing undulose extinction due to deformation stress (Fig. 4b). The effect of silicification decreases with distance from the auriferous quartz vein. Coarse pyrite crystals are recorded in the contact between silicified and carbonatized zones between the quartz grains and the calcite crystals (Fig. 4c). *Carbonatization* comprises calcite, dolomite, and ankerite as the essential alteration mineral constituents. Calcite

Fig. 5 Photomicrographs showing arsenopyrite idiomorphic rhombohedral crystals and massive aggregates invaded by later chalcopyrite (a), idiomorphic pyrite crystals filling microfractures within quartz and dendritic pyrite recorded in the alteration zone (b), pyrite displaying dendritic texture (c), fine gold grains within and around pyrite crystal in quartz vein (d), fine gold disseminations in alteration zone (e), sphalerite aggregates invading chalcopyrite (f), bent sphalerite reflecting ductile deformation (g), and galena granular aggregates commonly altered to anglesite and overlapping pyrrhotite (h). *Ccp* chalcopyrite, *Apy* arsenopyrite, *Dendr. Py.* dendritic pyrite, *W. Mfr.* wide microfracture, *Pan. Py* panidiomorphic pyrite, *Dis.* disseminated, *Sp* sphalerite, *Car.* carbonate, *Po* pyrrhotite, *Gn* galena, *Ang* anglesite



occurs locally as aggregates. Fine- to coarse-grained opaque phases, most probably sulfide minerals, occur within calcite aggregates (Fig. 4d). In places, calcite shows perfect characteristic cleavage. Parallel calcite crystals represent two birefringence shadows due to displacement in its crystallographic orientation. Dolomite is widely spread among the wall rock alteration zones. It is found as equigranular medium-grained crystals of ideal rhombohedral shape disseminated in the metavolcanoclastic rocks (Fig. 4e).

Ankerite and antigorite are recorded as relict grains. The coarse ankerite grains are surrounded by brown staining rims (Fig. 4f). *Chloritization* is observed in both the mineralized zones and the host rocks. Chlorite forms flakes and aggregates filling spaces between the quartz and the carbonate minerals (Fig. 4g). Chlorite exists within the veins and veinlets. Both carbonatization and chloritization show general decrease with depth. *Sericitization* is the essential alteration process responsible for precipitation of most of the

Table 1 Microprobe analysis (in wt%) of native gold grains, Dungash gold mine

Sample no.	A1	A2	A4	B2	B3	C4	C2	C3	C5	C6	C8	C9	C10	Av. n = 13
Au	79.63	79.64	80.03	79.76	79.46	79.13	80.48	78.9	79.08	79.9	80.48	80.34	79.96	79.75
Ag	20.53	20.87	20.79	20.5	21.5	21.1	20.05	20.82	20.86	20.04	19.76	19.67	19.41	20.45
S	0.05	0.1	0.05	0.05	0.05	0.13	0.05	0.05	0.1	0.13	0.05	0.1	0.13	0.08
Fe	0.05	0.05	0.05	0.07	0.016	0.15	0.66	0.72	0.05	0.05	0.05	0.55	0.92	0.32
Total	100.3	100.7	100.9	100.4	101	100.5	101.2	100.5	100.1	100.1	100.3	100.7	100.4	100.6
Au/Ag	3.9	3.8	3.9	3.9	3.7	3.8	4	3.8	3.8	4	4.1	4.1	4.1	3.9
Log Au/Ag	0.59	0.58	0.59	0.59	0.57	0.58	0.6	0.58	0.58	0.6	0.62	0.62	0.62	0.59
Au fineness ‰	795	792	794	796	787	790	801	791	791	800	803	803	805	795

sulfides. Usually, it is represented by fine-grained acicular sericite. *Argillic alteration* is less abundant and composed of sericite, kaolinite, pyrophyllite, and chlorite. *Sericitization* is pervasive and typically better developed alteration zone at the contact with the auriferous quartz vein. *Sulfidation* is recorded intercalating the other alteration types as thin crustation. Sulfides occur as dispersed grains commonly associated with sericite and quartz (Fig. 4h). Sulfidation is an important hydrothermal wall rock alteration, as it is a gold carrier. *Ferruginization* is recorded along fractures in the alteration zones. It is characterized by the reddish color and existence of sulfide minerals (Fig. 3c). Ferruginization

is also recorded by brown staining surrounding the carbonate minerals (Fig. 4f).

Ore minerals

The recorded primary ore mineral assemblage comprises native gold, arsenopyrite, pyrite, pyrrhotite, sphalerite, chalcopyrite, and galena. The secondary minerals are anglesite and goethite. *Arsenopyrite* is very dominant in samples of the auriferous quartz veins, especially those collected from underground workings. Arsenopyrite is the first precipitated sulfide

Table 2 Microprobe analysis of arsenopyrite grains, Dungash gold mine

Sample no.	E1	E3	E2	A6	A1	B	B3	A4	A1	Av. (n = 9)
Wt%										
Fe	34.83	34.02	33.96	34.35	33.58	35.8	35.55	35.34	35.58	34.77
S	22.91	20.43	20.81	21.22	23.73	24.68	23.92	24.52	23.53	22.86
As	40.17	43.3	42.93	43.03	41.06	37.35	38.35	37.13	39.17	40.27
Co	0.05	0.05	0.05	0.05	0.05	0.12	0.23	0.42	0.21	0.13
Au	0.22	0.05	0.13	0.05	0.05	0.05	0.12	0.05	0.05	0.08
Sum	98.18	97.85	97.88	98.70	98.47	98.00	98.17	97.46	98.54	98.11
Atomic %										
Fe	33.24	33.37	33.20	33.20	31.80	33.53	33.52	33.30	33.57	33.19
S	38.08	34.91	35.44	35.73	39.15	40.27	39.29	40.24	38.68	38.01
As	28.57	31.66	31.28	31.00	28.99	26.08	26.95	26.08	27.55	28.66
Co	0.05	0.05	0.05	0.05	0.04	0.11	0.21	0.37	0.19	0.12
Au	0.06	0.01	0.04	0.01	0.01	0.01	0.03	0.01	0.01	0.02
Sum	100	100	100	100	100	100	100	100	100	100
Formula										
Fe	1.00	1.00	1.00	1.00	0.95	1.01	1.01	1.00	1.01	1.00
S	1.14	1.05	1.06	1.07	1.17	1.21	1.18	1.21	1.16	1.14
As	0.86	0.95	0.94	0.93	0.87	0.78	0.81	0.78	0.83	0.86
Co	0.00	0.00	0.00	0.00	0.00	0.00	0.01	0.01	0.01	0.00
Au	0.00	0.00	0.00	0.00	0.00	0.00	0.00	0.00	0.00	0.00
Sum	3	3	3	3	3	3	3	3	3	3

Table 3 Microprobe analysis of pyrite, Dungash gold mine

Sample no.	A	A1	B2	B3	C4	C5	C6	D7	D2	E5	E2	Av. (n = 11)
Wt%												
Fe	45.51	45.85	46.02	45.91	46.08	44.14	45.15	45.52	45.92	45.28	45.56	45.54
S	53.04	53.35	53.46	53.5	54.14	52.81	53.98	52.19	52.38	51.69	53.17	53.06
As	0.05	0.05	0.61	0.63	0.65	0.05	0.05	0.06	0.05	0.05	0.05	0.21
Co	0.37	0.05	0.05	0.05	0.05	0.05	1.48	0.05	0.05	0.05	0.05	0.21
Ni	0.65	0.55	0.05	0.05	0.05	0.17	0.3	0.3	0.75	0.05	0.05	0.27
Cu	0.05	0.05	0.05	0.05	0.05	0.11	0.1	0.05	0.05	0.05	0.05	0.06
Au	0.05	0.05	0.05	0.05	0.05	0.11	0.15	0.05	0.05	0.05	0.05	0.06
Sum	99.72	99.95	100.29	100.24	101.07	97.44	101.21	98.22	99.25	97.22	98.98	99.41
Atomic %												
Fe	32.75	32.88	32.93	32.86	32.67	32.34	32.01	33.26	33.27	33.41	32.93	32.85
S	66.49	66.64	66.64	66.70	66.87	67.39	66.67	66.42	66.11	66.45	66.94	66.66
As	0.03	0.03	0.33	0.34	0.34	0.03	0.03	0.03	0.03	0.03	0.03	0.11
Co	0.25	0.03	0.03	0.03	0.03	0.03	0.99	0.03	0.03	0.03	0.03	0.14
Ni	0.44	0.38	0.03	0.03	0.03	0.12	0.20	0.21	0.52	0.04	0.03	0.19
Cu	0.03	0.03	0.03	0.03	0.03	0.07	0.06	0.03	0.03	0.03	0.03	0.04
Au	0.01	0.01	0.01	0.01	0.01	0.02	0.03	0.01	0.01	0.01	0.01	0.01
Sum	100	100	100	100	100	100	100	100	100	100	100	100
Formula												
Fe	0.98	0.99	0.99	0.99	0.98	0.97	0.96	1.00	1.00	1.00	0.99	0.99
S	1.99	2.00	2.00	2.00	2.01	2.02	2.00	1.99	1.98	1.99	2.01	2.00
As	0.00	0.00	0.01	0.01	0.01	0.00	0.00	0.00	0.00	0.00	0.00	0.00
Co	0.01	0.00	0.00	0.00	0.00	0.00	0.03	0.00	0.00	0.00	0.00	0.00
Ni	0.01	0.01	0.00	0.00	0.00	0.00	0.01	0.01	0.02	0.00	0.00	0.01
Cu	0.00	0.00	0.00	0.00	0.00	0.00	0.00	0.00	0.00	0.00	0.00	0.00
Au	0.00	0.00	0.00	0.00	0.00	0.00	0.00	0.00	0.00	0.00	0.00	0.00
Sum	3	3	3	3	3	3	3	3	3	3	3	3

mineral. It commonly occurs as idiomorphic rhombohedral crystals and as massive aggregates. The mineral is usually invaded by the later chalcopyrite (Fig. 5a). *Pyrite* is the main

sulfide mineral and occurs in a range of habits. The common habits of pyrite are idiomorphic crystals filling microfractures (Fig. 5b) and branching pyrite displaying dendritic texture

Table 4 Microprobe analysis of pyrrhotite, Dungash gold mine

Sample no.	A1	A2
Wt%		
Fe	58.65	58.92
S	39.17	38.98
Ni	0.64	0.21
Ag	0.14	0.05
Sum	98.60	98.16
Atomic %		
Fe	45.98	46.38
S	53.49	53.45
Ni	0.48	0.16
Ag	0.06	0.02
Sum	100	100
Formula		
Fe	0.92	0.93
S	1.07	1.07
Ni	0.01	0.00
Ag	0.00	0.00
Sum	2	2

Table 5 Microprobe analysis of sphalerite, Dungash gold mine

Sample no.	A1	A2	B2	B3	Av. (n = 4)
Wt%					
Fe	5.83	5.79	5.63	5.75	5.75
S	33.04	33.23	33.19	32.72	33.05
Cu	0.25	0.05	0.15	0.22	0.17
Zn	58.33	58.18	58.55	58.27	58.33
Sum	97.45	97.25	97.52	96.96	97.3
Atomic %					
Fe	5.14	5.10	4.96	5.10	5.06
S	50.74	51.03	50.89	50.56	50.81
Cu	0.19	0.04	0.12	0.17	0.13
Zn	43.93	43.82	44.03	44.16	43.99
Sum	100	100	100	100	100
Formula					
Fe	0.10	0.10	0.10	0.10	0.10
S	1.01	1.02	1.02	1.01	1.02
Cu	0.00	0.00	0.00	0.00	0.003
Zn	0.88	0.88	0.88	0.88	0.88
Sum	2	2	2	2	2

Table 6 Microprobe analysis of chalcopyrite, Dungash gold mine

Sample no.	E1	E3	E2	A	A1	B	B4	Av. (n = 7)
Wt%								
Fe	29.55	29.88	29.29	30.18	29.33	29.38	29.27	29.55
S	34.54	34.51	34.43	34.56	34.55	34.78	34.36	34.53
Cu	33.56	33.66	32.99	34.22	33.42	33.38	33.71	33.56
Ag	0.13	0.05	0.05	0.05	0.05	0.05	0.05	0.06
Sum	97.78	98.10	96.76	99.01	97.35	97.59	97.39	97.71
Atomic %								
Fe	24.77	24.98	24.76	25.05	24.66	24.62	24.64	24.79
S	50.44	50.26	50.70	49.97	50.61	50.77	50.39	50.45
Cu	24.73	24.74	24.51	24.96	24.70	24.59	24.94	24.74
Ag	0.06	0.02	0.02	0.02	0.02	0.02	0.02	0.03
Sum	100	100	100	100	100	100	100	100
Formula								
Fe	0.99	1.00	0.99	1.00	0.99	0.98	0.99	0.99
S	2.02	2.01	2.03	2.00	2.02	2.03	2.02	2.02
Cu	0.99	0.99	0.98	1.00	0.99	0.98	1.00	0.99
Ag	0.00	0.00	0.00	0.00	0.00	0.00	0.00	0.00
Sum	4	4	4	4	4	4	4	4

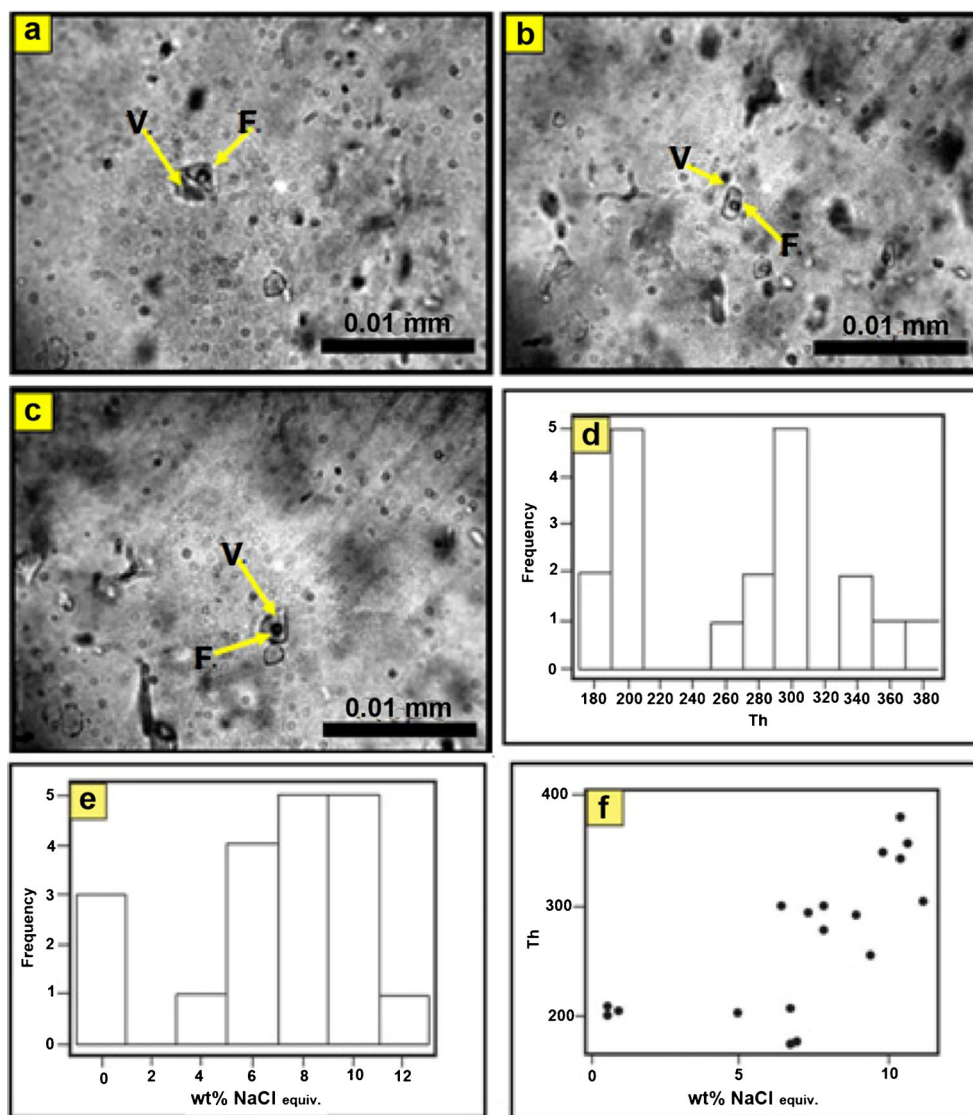
(Fig. 5c). The peripheries of pyrite are commonly altered to a Ni-rich zone (EMP analysis) and form a girdle-band texture. The mineral has direct contact and textural relationships with all the ore minerals including gold. *Native gold* occurs as fine grains and specks inside and around the sulfide minerals, especially pyrite (Fig. 5d), and as very fine-grained disseminations and inclusions (Fig. 5e). The first form is recorded only in the quartz veins while the second one exists in the wall rock alteration zones. Both forms belong to the same phase of deposition. *Pyrrhotite* crystals occasionally occur as subordinate

discrete grains of medium size with irregular or triangular shape crystals overlapped by galena. *Sphalerite* exists as granular aggregates with irregular outlines invading chalcopyrite (Fig. 5f). It seems that the zone of precipitation was subjected to ductile deformation as indicated by presence of bent elongated sphalerite crystals (Fig. 5g). *Chalcopyrite* occurs as fine- to medium-grained irregular aggregates. It usually invades arsenopyrite (Fig. 5a). Remnants of chalcopyrite are recorded also inside and/or replaced by sphalerite (Fig. 5f). *Galena* occurs as granular masses with xenomorphic

Table 7 Paragenetic sequence of ore minerals in the Dungash gold deposit

Ore Mineral	Sequence of deposition	Supergene
Arsenopyrite	-----	
Pyrite	-----	
Gold	-----	
Pyrrhotite	-----	
Chalcopyrite	-----	
Sphalerite	-----	
Galena	-----	
Anglesite		-----
Goethite		-----

Fig. 6 **a** Photomicrograph of primary negative crystal two-phase (fluid–vapor) aqueous inclusions in quartz. Notice secondary inclusions along a healed fracture at the right of the photo. **b, c** Photomicrograph of primary two-phase (fluid–vapor) aqueous inclusion in quartz. **d** Histogram of homogenization temperatures for primary fluid inclusions in quartz. **e** Histogram of salinity for primary fluid inclusions in quartz. **f** Homogenization temperatures vs. salinity in primary fluid inclusions in quartz



peripheries. Galena overlaps pyrrhotite pointing to its deposition after pyrrhotite. It is commonly altered to anglesite (Fig. 5h). *Anglesite* exists as an oxidation product of galena. *Goethite* is pseudomorph after pyrite.

The microprobe analysis (EMP) analysis of native gold grains recorded Ag as chief constituent (Table 1) with occasionally presence of S and Fe. The latter is probably due to the groundmass. The contents of Au are between 78.9 and 80.48 wt%, those of Ag between 19.41 and 21.5 wt%. Arsenopyrite belongs to the sulfarsenides group (FeAsS–CoAsS–NiAsS). The studied arsenopyrite is characterized by gold contents varying from 0.05 to 0.22 wt% and Co content up to 0.42 wt% while Ni is below the detection limit (Table 2). The studied pyrite is characterized by gold contents up to 0.15 wt%, Co 1.48 wt%, Ni 0.75 wt%, As 0.63 wt%, and Cu 0.11 wt% (Table 3). Table 4 shows that pyrrhotite contains traces of silver (up to 0.14 wt%) and Ni (up to 0.64 wt%). Table 5 shows that sphalerite contains impurities of Fe (up to

5.83 wt%) and Cu (up to 0.25 wt%). The analyzed chalcopyrite crystals do not show any significant compositional differences and contain up to 0.13 wt% Ag (Table 6).

The microprobe analysis (EMP) recorded high fineness gold grains (Table 1). Moreover, Au was detected in pyrite and arsenopyrite (Tables 2 and 3). Cobalt was detected in arsenopyrite and pyrite, Ni in pyrrhotite and pyrite (Tables 2, 3 and 4).

Based on the mutual textural relationships and crystal morphology of the ore minerals, the paragenesis of deposition of these minerals (Table. 7) is that the primary gold and sulfide minerals were deposited during the emplacement of the quartz veins and hydrothermal alteration of the wall rocks while goethite and anglesite represent a supergene stage. Cataclastic deformation and shearing forces resulted in intensive fracture systems. Hydrothermal As–Fe-bearing solutions leaching both Ni and Co from the ultramafic source rocks acted along these fractures. This led to

Table 8 Chemical composition of the host rocks and quartz veins, Dungash gold mine

Rock type	Host rocks										Quartz veins	
	Sample no.	300	301	306	307	308	309	310	311	321	322	304
Major oxides (wt%)												
SiO ₂	63.75	63.7	63.83	63.9	61	61.1	62.62	63.81	59.04	65.78	88.19	84.76
TiO ₂	0.71	0.66	0.72	0.8	0.56	0.85	0.99	0.81	1.15	1.09	0.02	0.04
Al ₂ O ₃	15.61	15.5	15.26	15.53	14.76	16.05	15.85	14.69	17.04	15.34	5.13	6.15
FeO*	3.12	3.12	3.09	2.97	7.07	8.01	8.34	7.85	6.05	5.28	0.39	0.53
MnO	0.15	0.14	0.15	0.15	0.17	0.19	0.22	0.2	0.18	0.08	0.05	0.03
MgO	1.63	1.8	1.72	1.64	4.7	4.61	4.44	4.92	5.43	1.93	0.10	0.13
CaO	4.62	4.65	4.51	4.65	2.59	2.13	2.18	1.66	2.29	0.74	2.19	4.69
Na ₂ O	2.63	2.77	2.63	2.61	3.6	3.72	1.55	2.74	1.67	0.85	1.79	1.24
K ₂ O	1.51	1.41	1.51	1.5	2.53	0.76	1.04	1.36	3.93	6.13	0.16	0.53
P ₂ O ₅	0.22	0.25	0.26	0.26	0.19	0.23	0.2	0.11	0.22	0.17	0.11	0.09
LOI	5.61	5.32	5.83	5.62	2.43	2.03	2.16	1.46	2.60	2.08	1.11	1.42
Total	99.56	99.32	99.51	99.63	99.6	99.68	99.59	99.61	99.6	99.47	99.24	99.61
Trace elements (ppm)												
Ba	402	502	415	428	456	45	16	53	693	820	126	291
Rb	85	67	72	77	62	12	6	5	51	5	244	171
Sr	601	594	598	574	562	170	139	201	178	105	221	191
Y	13	14	15	19	15	7	6	–	22	12	8	6
Zr	139	170	153	151	161	55	41	75	356	80	80	76
Nb	9	13	12	8	10	–	2	–	7	–	105	116
Pb	16	14	10	12	15	47	40	48	17	20	31	45
Zn	68	76	69	66	73	57	33	30	179	20	168	182
Cu	30	25	20	24	18	95	95	85	16	30	151	114
Ni	25	32	36	42	17	63	50	42	82	91	3	1
V	48	65	62	52	51	63	28	53	108	33	9	11
Cr	60	68	73	66	76	42	41	50	148	107	3	1
Co	19	10	17	14	20	–	20	2	19	35	3	3
Au	–	–	–	–	–	–	–	–	–	–	3.62	2

– below lower limit of detection

*All Fe₂O₃ calculated as FeO

deposition of arsenopyrite, pyrite, and pyrrhotite in the quartz veins along the fracture systems as well as formation of the mineralized wall rock alteration zones. Gold was deposited as separated grains in the quartz vein and as minute inclusions in pyrite and arsenopyrite. Then chalcopyrite, sphalerite, and galena were deposited.

Accordingly, from these statements, the paragenetic sequence of ore minerals considering slow rate of decrease of temperature is as in Table 7.

Fluid inclusions

Using cryo- and thermometric methods, the following characteristics of fluid inclusions in the auriferous quartz samples

were determined: (a) the freezing point depression temperatures, (b) the concentration of solution, (c) the eutectic temperature, (d) the homogenization temperatures, (e) the fluid density, and (f) the pressure.

The size of fluid inclusions ranges from <5 to 30 μm. Taking into consideration several features, the inclusions are classified into two chief types. The first is a simple fluid enriched two-phase (fluid–vapor) inclusions of dimensions from 5 to 30 μm and contain approximately 10 to 50 vol% of gas. They are rare and have oval, wedge-shaped or negative crystal forms (Fig. 6a–c). They occur isolated or in intergranular groups. Their shape and spatial distribution indicate, following the criteria of Roedder (1984), their primary origin. The second type, the most abundant, is secondary two-phase aqueous (fluid–vapor) inclusions. They are concentrated

Table 9 Chemical composition of the different alteration zones, Dungash gold mine

Alteration type	Carbonatized zone						Chloritized zone				Sericitized zone			
	313	315	316	317	318	Av.	312	319	320	Av.	302	303	305	Av.
Sample no.	313	315	316	317	318	Av.	312	319	320	Av.	302	303	305	Av.
Major oxides (wt%)														
SiO ₂	58.06	57.3	59.51	59.06	58.91	58.56	58.74	59.44	58.14	58.77	64.08	62.54	62.87	63.16
TiO ₂	1.04	1.09	1.09	1.13	1.1	1.09	1.35	1.32	1.19	1.28	1.11	1.04	1.03	1.06
Al ₂ O ₃	16.08	15.3	13	15.11	14.98	14.89	8.24	10.77	11.08	10.03	16.06	16.35	14.28	15.56
FeO*	4.15	3.88	5.84	3.86	4.48	4.44	13.31	13.53	13.18	13.33	2.89	4.65	5.02	4.18
MnO	0.17	0.13	0.12	0.11	0.15	0.13	0.13	0.15	0.21	0.16	0.12	0.23	0.1	0.15
MgO	3.3	2.88	2.88	3.87	3.69	3.32	6.58	7.43	6.52	6.84	0.87	1.34	2.77	1.66
CaO	9.42	9.84	6.91	9.76	8.79	8.94	2.81	1.44	2.11	2.12	1.71	1.62	1.82	1.71
Na ₂ O	2.71	4.11	4.04	2.41	2.6	3.17	1.14	0.67	1.03	0.94	4.05	4.44	4.11	4.2
K ₂ O	1.94	2.58	2.61	1.88	1.64	2.13	1.62	0.5	2	1.37	5.5	5.12	5.65	5.42
P ₂ O ₅	0.22	0.29	0.26	0.22	0.25	0.24	0.25	0.22	0.17	0.21	0.22	0.19	0.12	0.17
LOI	2.51	2.21	3.16	2.18	2.98	2.60	5.21	3.84	3.78	4.27	3.02	2.04	1.77	2.27
Total	99.6	99.61	99.42	99.59	99.57	99.51	99.38	99.31	99.41	99.32	99.63	99.56	99.54	99.54
Trace elements (ppm)														
Ba	11	10	12	11	10	10.8	9	6	8	7.66	13	25	23	20.33
Rb	60	74	66	68	63	66.2	80	107	91	92.66	96	7	25	42.66
Sr	587	601	605	601	578	594.4	598	623	609	610	604	139	187	310
Y	28	27	17	26	21	23.8	29	17	23	23	21	10	4	11.66
Zr	356	367	347	361	355	357.2	371	306	356	344.3	298	75	65	146
Nb	8	9	11	12	10	10	8	4	9	7	5	4	3	4
Pb	14	13	10	11	15	12.6	12	35	26	24.33	54	18	54	42
Zn	197	169	188	188	199	188.2	174	199	181	184.7	208	25	45	92.66
Cu	15	17	22	18	21	18.6	21	19	23	21	25	32	124	60.33
Ni	44	48	55	50	53	50	51	66	71	62.66	75	35	64	58
V	124	100	99	101	112	107.2	111	152	136	133	143	42	33	72.66
Cr	154	146	136	145	151	146.4	153	210	190	184.3	168	70	52	96.66
Co	27	22	30	27	31	27.4	20	15	21	18.66	18	29	16	21
Au	0.42	6	13.4	11.6	0.3	6.344	--	--	--	--	0.21	0.36	0.1	0.22

– below lower limit of detection

*All Fe₂O₃ calculated as FeO

along or near healed fractures and display oval or elongated shape (Fig. 6a). Their linear dimensions reach up to 50 μm with 5–90 vol% of gas.

Although direct physical contact of fluid inclusions with gold grains was not observed, gold grains are intergrown with quartz in the vein and the primary fluid inclusions may represent either quartz-forming fluids and/or the gold-bearing fluids. Therefore, microthermometric determinations were made only on the primary inclusions. These inclusions homogenize to a liquid phase at homogenization temperatures ranging from 380 to 177 °C (Fig. 6d). This range of temperature favors that these fluid inclusions are the residual fluids of the quartz-forming hydrothermal fluids. The final melting temperatures of ice range from –0.3 to –7.6 °C. The inclusions contain solutions

of wide range of salinity from 0.5 to 11.22 wt% NaCl_{equiv} (Fig. 6e) and a density of 0.4–0.97 g/cm³

The inclusions contain two types of solutions according to the degree of salinity. The first is low-salinity fluids (<1 wt% NaCl_{equiv}) with a density of 0.86 g/cm³. They homogenize over a narrow temperature range of 209 to 204 °C. The minimum pressure of trapping is 350 bars. The measured eutectic temperatures (T_e) in these inclusions range from –22 to –30 °C. These values of T_e are typical for the solution of Na and K chloride (Schiffries 1990). The second is moderately saline fluids (5–11.2 wt% NaCl_{equiv}) with a density of 0.76–0.93 g/cm³ which are the dominant. They homogenize over a temperature range of 177 to 380 °C. The minimum pressures of trapping are between 350 and 400 bars. The measured eutectic temperatures

Fig. 7 a–c Distribution curves of the chemical components of Dungash gold-bearing quartz vein, wall rock alteration zone, and host rocks along profile I. *Hr* host rock, *Ser* sericitized zone, *Qz V.* quartz vein

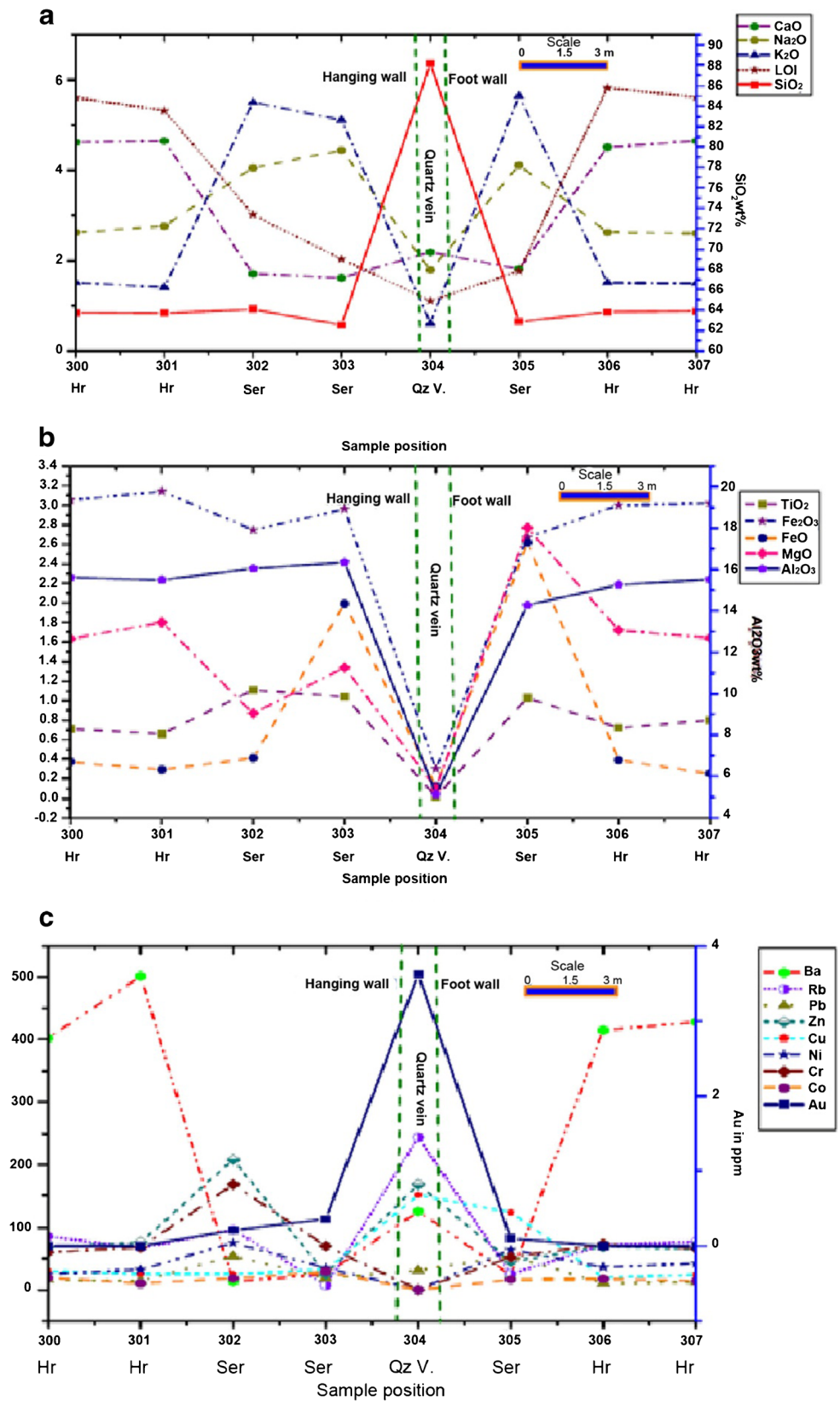


Fig. 8 a–d Distribution curves of the chemical components of Dungash gold-bearing quartz vein, wall rock alteration zones, and host rocks along profile II. *Chlo* chloritization, *Carb* carbonatization, *Q.V.* quartz vein, *Hr* host rocks

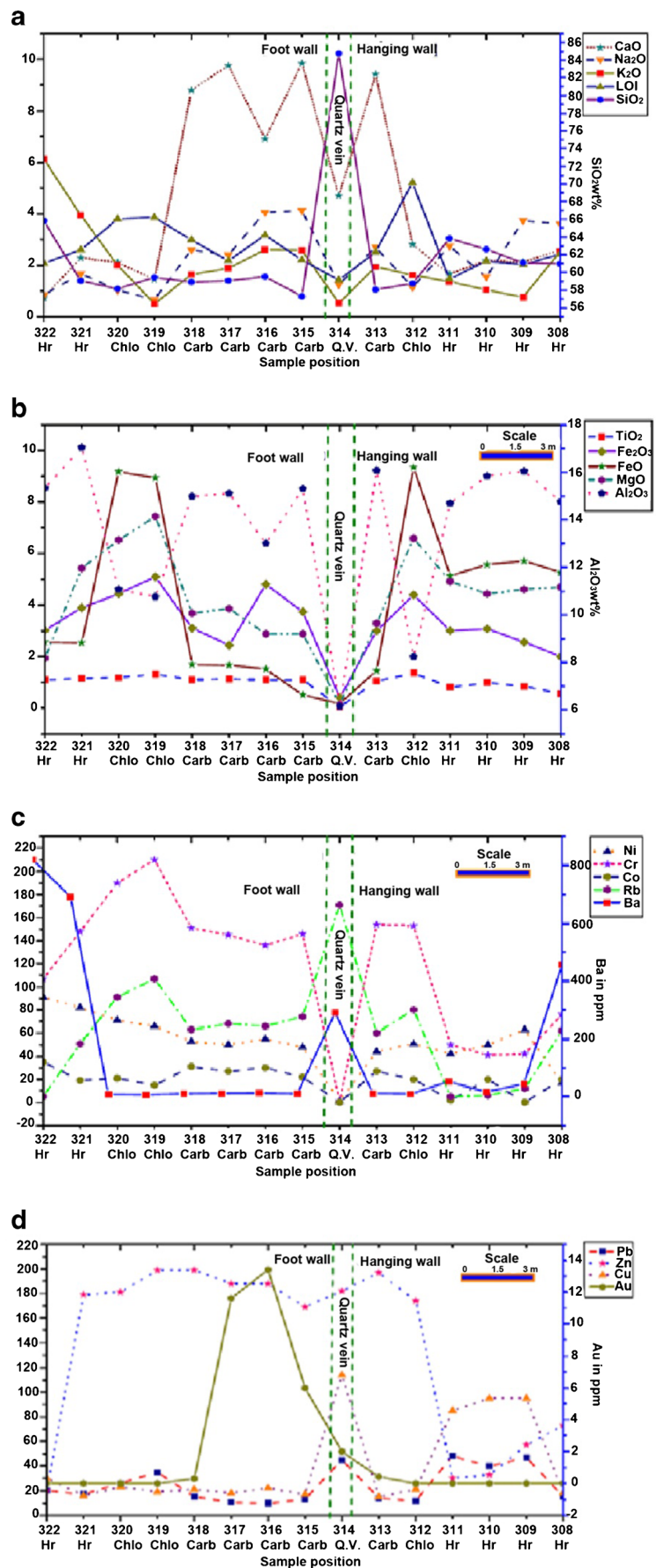


Table 10 Characteristic mineralogy and dominance of elements in the three principle alteration zones at the Dungash gold mine

Type of alteration	Mineral constituents	Characteristic oxides and trace elements
Chloritization	Chlorite, tremolite, hornblende, calcite, sericite, muscovite, pyrite, arsenopyrite, pyrrhotite	FeO, MgO, Fe ₂ O ₃ , TiO ₂ , LOI, Rb, Zn, Cr, Co
Sericitization	Kaolinite, sericite, epidote, chlorite, quartz, calcite, albite, pyrite, arsenopyrite	K ₂ O, Na ₂ O, FeO, TiO ₂ , Pb, Zn, Cu, Ni, Cr, Co, Au
Carbonatization	Calcite, dolomite, ankerite, quartz, sericite, talc, albite, antigorite, magnesite, pyrite, arsenopyrite	CaO, Fe ₂ O ₃ , Na ₂ O, K ₂ O, Zn, Cr, Co, Rb, Au

in these inclusions range from -35 to -40 °C and characterize chloride solutions with Fe, Mg, and Na cations.

The fluid evolution in the auriferous quartz vein of Dungash is shown in Fig. 6f, where a crude linear trend in temperature versus salinity is observed. The recorded low salinity and low-temperature fluid is likely to reflect meteoric waters. The trend of fluid evolution during deposition is a direct consequence of fluid mixing, whereby the proportion of moderately saline, high-temperature magmatic hydrothermal fluid was initially higher and then decreased during the later stages of deposition as the hydrothermal system progressively mixed with cooler, low-salinity waters.

Distribution patterns of gold and chemical components

Two profiles traversing the wall rock alterations associating the auriferous quartz veins as well as the host rocks were sampled. The first profile (I) cuts the mineralized quartz vein and the sericitized zone. The second profile (II) is crossing the main lode associated with chloritized and carbonatized zones. The results of chemical analysis of the major and trace element concentrations of the collected samples from both profiles are given in Tables 8 and 9 and plotted in Figs. 7 and 8. Table 10 represents the mineral constituents and the characteristic major element oxides and trace elements for the samples taken across the alteration zones.

1. The geochemical characteristics of each alteration zone are as follows:
 - (a) The sericitized zone is distinguished by comparatively low CaO, MgO, loss on ignition (LOI), and high K₂O, Na₂O, and TiO₂ contents (Fig. 7a, b).
 - (b) The carbonatized zone is distinguished by comparatively low SiO₂, MgO, FeO, and high CaO and Na₂O (Fig. 8a, b). The CaO, MgO, and LOI contents point to presence of calcite and dolomite.

- (c) The chloritized zone shows a relatively higher MgO than CaO (Table 9), high FeO^t, and low Al₂O₃.
2. The plotted distribution curves of the major element oxides and trace elements in relation to that of the gold show the following characteristics:
 - (a) Gold, Pb, Zn, Ni, and Cr appear concentrated in the sericitized zone relative to the host rock (Fig. 7c).
 - (b) The highest gold contents are recorded in the carbonatized zones of the footwall. Its content in this zone exceeds several times its content in the quartz vein (Fig. 8c). The distribution of Cr and Zn is partially related to that of the CaO and vice versa for Cu and Pb.
 - (c) Cu and Pb are concentrated in the quartz vein compared to the alteration zones.

Discussion

Hassaan (2006, 2011) recorded the relationship between the increased content of the major element oxides of several alteration types and the chief alteration minerals. Moreover, the similar distribution of gold and several associated trace elements, for example, silver, arsenic..., etc., and the characteristic major oxides forming the chief alteration minerals in each alteration type are recorded. He mentioned presence of relation between the formation temperature of one or more of the alteration minerals with the deposition temperature of gold and accumulation of both at the same site. Dolomite, ankerite, and calcite share gold (200 °C) its temperature of deposition explaining its accumulation chiefly in the carbonatized zone of the study area rather than in the quartz vein itself.

Microthermometric fluid inclusion analysis revealed that ores of the Dungash area formed from a moderately saline solution (5 to 11.22 wt% NaCl_{equiv}) with a density of 0.76–0.93 g/cm³ at temperatures above the recorded homogenization temperatures (T_h), which range from 380 to 177 °C. The minimum pressures of trapping are between 350 and 400 bars.

The variations in the chemical composition of minerals are due to the different physicochemical conditions of their formation, composition of ore-forming solutions, their redox potential, and acidity–alkalinity regime and to the chemical activities of sulfur and other elements. Therefore, the chemical composition of ore minerals is of special interest as it might serve as an indicator of the physicochemical conditions of ore formation and evolution of hydrothermal solutions (Pal'yanova et al. 2016). Also, as in the papers (Kretschmar and Scott 1976; Zharikov and Rusinov 1998; Pal'yanova 2008; Pal'yanova et al. 2016), the compositions of arsenopyrite, Fe–sphalerite, native gold, and mineral assemblages were used to estimate the physicochemical parameters of ore formation, namely T , fS_2 , and pH.

Au–Ag solid solutions are characterized by a wide variation in chemical compositions commonly expressed as the gold fineness ($1000 \times \text{Au}/(\text{Au} + \text{Ag})$, by wt%) (e.g., Morrison et al. 1991; Pal'yanova 2008). The gold fineness varies from 789 to 805‰ (Table 1) according to which the Au–Ag alloys correspond to high fineness gold or Au-rich electrum (Pal'yanova and Kolonin 2007). Pal'yanova (2008) examined the detailed physicochemical conditions for equilibria of the Au–Ag solid solutions and fluids. On the other hand, Au–Ag solid solutions of high gold finenesses have been reported from various types of Au–Ag deposits (e. g., Shikazono and Shimizu 1987; Morrison et al. 1991; Liang 2015; Liang and Hoshino 2015).

Application of Pal'yanova (2008) physicochemical modeling using gold fineness and Au/Ag ratios indicates that native gold (fineness = 800) at the conditions of Py–Po (–Mt) buffer at 1000 bar corresponds to a maximum temperature of 400 °C.

Application of Kretschmar and Scott's (1976) geothermometer indicates that arsenopyrite intergrown pyrrhotite and pyrite contains up to 31.66 at.% As, which corresponds to a maximum temperature of 380 °C and $\log 10/fS_2$ of –8 (Kretschmar and Scott 1976). The temperature agrees with the results of the studies of fluid inclusions.

According to Zharikov and Rusinov (1998), pH of ore-forming solutions varies from 2.0 to 7.5, depending on the type of metasomatic alterations of the host rocks. Metasomatic alteration assemblage in the ore zones of orogenic gold deposit represented by sericite–carbonate–chlorite is characterized by pH as great as 5–8 (Groves et al. 1998). The pH of ore-forming solutions of the wall rock alterations near veins in the Dungash area varies from 5 to 8.

Impurities in native gold (Fe and S), sphalerite (Cu), pyrrhotite (Ni and Ag), chalcopyrite (Ag), arsenopyrite (Co), and pyrite (As, Co, Ni, Cu) are very small, generally less than 1 wt% percent. Therefore, it is likely that these elements do not affect the thermochemical properties of host minerals. The recorded Co in the arsenopyrite grains, Co, and Ni in the pyrite as well as Ni in pyrrhotite grains may point to leaching by hydrothermal fluids from ultramafic source rocks.

Conclusions

1. At Dungash gold deposit, the recorded alteration processes acting on the wall rocks are represented by sericitization, argillic alteration, silicification, carbonatization, chloritization, sulfidization, ferrugination, and listwanitization.
2. The recorded ore mineral assemblage forming Dungash gold deposit is arsenopyrite, pyrite, native gold, pyrrhotite, sphalerite, chalcopyrite, and galena. These primary sulfide minerals were formed during the hydrothermal stage while anglesite and goethite represent the supergene stage.
3. The recorded Co in the arsenopyrite grains, Co, and Ni in the pyrite as well as Ni in pyrrhotite grains may point to leaching by hydrothermal fluids from ultramafic source rocks.
4. Microthermometric fluid inclusion analysis revealed that auriferous quartz precipitated from a moderately saline (up to 11.22 wt% NaCl_{equiv}) solution at temperatures above the recorded homogenization temperatures (T_h), which range from 380 to 177 °C. The minimum pressures of trapping are between 350 and 400 bars. The fluid evolution during mineralization is explained by mixing of a magmatic fluid with meteoric waters. Initially, the high temperature and moderately saline magmatic fluid dominated and became progressively diluted with meteoric waters.
5. The highest gold content is recorded in the carbonatized zone and the quartz veins. However, gold content in the carbonatized zone of the footwall exceeds several times its content in the quartz veins and the carbonatized zone of the hanging wall.
6. The alteration and shear zones are actually good new targets for gold deposits in the Eastern Desert (e.g., Barramiya, Abu Marawat, El Beida). It is recommended that these alteration zones must be carefully examined in detail for gold mineralization. Geochemical bedrock surveys of these zones in all types and ages of the basement rocks must be undertaken for gold exploration.

Acknowledgements We thank Prof. U. Schüßler for his help with electron microprobe analyses. Parts of this study were conducted at the University of Würzburg during a visit by Islam, A. D. Thanks also for the financial support from the DAAD.

References

- Abdel-Tawab MM (1992) Gold exploration in Egypt from Pharaonic to modern times. *Zb1 GeolPaleonTeil1* 1:2721–2733
- Ahmed SE (2012) Application of remote sensing techniques on gold mineralization and exploration at Dungash and Samut mines, South Eastern Desert, Egypt. M. Sc. Thesis, Cairo University

- Brown PE (1989) FLINCOR: a microcomputer program for the reduction and investigation of fluid-inclusion data. *Am Mineral* 74(11–12): 1390–1393
- Groves DI, Goldfarb RJ, Gebre-Mariam M, Hagemann SG, Robert F (1998) Orogenic gold deposits: a proposed classification in the context of their crystal distribution and relationship to other gold deposits types. *Ore Geol Rev* 13:7–27
- Hassaan MM (2006) Gold deposits in Egypt: a renewing resources for national income, The Ninth Arab Conference for mineral Resources, 30 Oct., I. N. V. Jeddah, Kingdom of Saudi Arabia, Texts Book. 3: 45–42
- Hassaan MM (2011) Metallic ore deposits of the Nubian Shield in Egypt: tectonic environs, geochemical behavior, promising sites. LAP LAMBERT Academic Publishing Gmb H & Co. KG and licensors, 256
- Helba HA, Khalil IK, Abdou NM (2001) Alteration patterns related to hydrothermal gold mineralization in meta-andesites at Dungash area, Eastern Desert, Egypt. *Resource Geo* 151:19–30
- Khalil KI, Helba HA, Mucke A (2003) Genesis of the gold mineralization at the Dungash gold mine area, Eastern Desert, Egypt: a mineralogical-microchemical study. *J Afr Earth Sci* 37:111–122
- Kretschmar U, Scott SD (1976) Phase relations involving arsenopyrite in the system Fe–As–S and their application. *Can Mineral* 14:364–386
- Liang Y (2015) The mineralization of the Woxi Au–Sb–W deposit, western Hunan, China. Graduate School of Science, Hiroshima University, Hiroshima
- Liang Y, Hoshino K (2015) Thermodynamic calculations of $\text{Au}_x\text{Ag}_{1-x}$ —fluid equilibria and their applications for ore-forming conditions. *Appl Geochem* 52:109–117
- Marten BE (1986) Reconnaissance of the gold deposits of the Eastern Desert of Egypt. Part I inter. Rep., no. 39/1986. *Geol. Surv. Egypt, Cairo, Egypt*. 101P
- Morrison GW, Rose WJ, Jaireth S (1991) Geological and geochemical controls on the silver content (fineness) of gold in gold–silver deposits. *Ore Geol Rev* 6:333–364
- Pal'yanova GA (2008) Physicochemical modeling of the coupled behavior of gold and silver in hydrothermal processes: gold fineness, Au/Ag ratios and their possible implications. *Chem Geol* 255:399–413
- Pal'yanova GA, Kolonin GR (2007) Geochemical mobility of Au and Ag during hydrothermal transfer and precipitation: thermodynamic simulation. *Geochem Int* 45(8):744–757
- Pal'yanova GA, Savva NE, Zhuravkova TV, Kolova EE (2016) Gold and silver minerals in low-sulfidation ores of the Julietta deposit (northeastern Russia). *Russ Geol Geophys* 57:1171–1190
- Roedder E (1984) Fluid inclusions. In *Reviews in mineralogy* (ed. P. H. Ribbe). Mineral Soc Amer 12: 644P
- Schiffries CM (1990) Liquid-absent aqueous fluid inclusions and phase equilibria in the system CaCl_2 – NaCl – H_2O . *Geochemica et Cosmochemica Acta* 54:611–619
- Shikazono N, Shimizu M (1987) The Ag/Au ratio of native gold and electrum and the geochemical environment of gold vein deposits in Japan. *Mineral Deposita* 22:309–314
- Takla MA (2001) Gold mineralization in Egypt: an overview. The Mineralogical Society, Egypt, The 14th Annual Meeting (abstract)
- Zhang YG, Frantz JD (1987) Determination of the homogenization temperatures and densities of supercritical fluids in the system NaCl – KCl – CaCl_2 – H_2O using synthetic fluid inclusions. *Chem Geol* 64(3):335–350
- Zharikov VA, Rusinov VL (1998) *Metasomatism and metasomatic rocks* [in Russian]. Nauchnyi Mir, Moscow
- Zoheir B, Weihed P (2014) Greenstone-hosted lode-gold mineralization at Dungash mine, Eastern Desert, Egypt. *J Afr Earth Sci* 99(1):165–187
- Zoheir BA, El-Shazly AK, Helba H, Khalil KI, Bodnar RJ (2008) Origin and evolution of the Um Egat and Dungash orogenic gold deposits, Egyptian Eastern Desert: evidence from fluid inclusions in quartz. *Econ Geol* 103:405–424